Naval Surface Warfare Center
Carderock Division
West Bethesda, MD 20817-5700

NSWCCD-61-TR-2022/17 **September 2022**

Platform Integrity Department

Technical Report

Computational Simulation and Distortion Validation from Conventional and Synergic Processes of Gas Metal Arc Welding (GMAW)

by

Sean M. Orzolek

Charles R. Fisher

Computational Simulation and Distortion Validation from Conventional and Synergic Processes of Gas Metal Arc Welding (GMAW)

NSWCCD-61-TR–2022/17

Naval Surface Warfare Center
Carderock Division
West Bethesda, MD 20817-5700

NSWCCD-61-TR-2022/17 **September 2022**

Platform Integrity Department
Technical Report

Computational Simulation and Distortion Validation from Conventional and Synergic Processes of Gas Metal Arc Welding (GMAW)

by
Sean M. Orzolek
Charles R. Fisher

REPORT DOCUMENTATION PAGE

Form Approved OMB No. 0704-0188

1. REPORT DATE *(DD-MM-YYYY)*	2. REPORT TYPE	3. DATES COVERED *(From - To)*
17-09-2022	Technical Report	Mar 2021 – Jan 2022

4. TITLE AND SUBTITLE

Computational Simulation and Distortion Validation from Conventional and Synergic Processes of Gas Metal Arc Welding (GMAW)

5a. CONTRACT NUMBER N/A

5b. GRANT NUMBER N/A

5c. PROGRAM ELEMENT NUMBER N/A

6. AUTHOR(S)
Sean M. Orzolek
Charles R. Fisher

5d. PROJECT NUMBER N/A

5e. TASK NUMBER

5f. WORK UNIT NUMBER

7. PERFORMING ORGANIZATION NAME(S) AND ADDRESS(ES) AND ADDRESS(ES)
Naval Surface Warfare Center, Carderock Division
Code 611
9500 MacArthur Boulevard
West Bethesda, MD 20817-5700

8. PERFORMING ORGANIZATION REPORT NUMBER
NSWCCD-61-TR-2022/17

9. SPONSORING / MONITORING AGENCY NAME(S) AND ADDRESS(ES)
William Mullins
Program Manager, 332
Office of Naval Research
Arlington, VA 22217

10. SPONSOR/MONITOR'S ACRONYM(S)

11. SPONSOR/MONITOR'S REPORT NUMBER(S) N/A

12. DISTRIBUTION / AVAILABILITY STATEMENT
Distribution A. Approved for public release; distribution unlimited.

13. SUPPLEMENTARY NOTES

14. ABSTRACT:
The Welding, Processing, and Nondestructive Evaluation (NDE) Branch (Code 611) at the Naval Surface Warfare Center, Carderock Division (NSWCCD) was tasked with developing a digital twin of an experimental welding study to evaluate the residual stress and distortion of aluminum B2V.1 joints. The intent of the study was to validate the computational welding model, developed using a welding-based finite element analysis (FEA) software called SYSWELD, through the comparison of predicted and measured distortion values. However, the previous study that provided the experimental basis of this work did not include all of the information necessary for model validation, and the large number of assumptions made in the model, which resulted in inaccurate predictions. This study provides an example of the limitation of computational modeling when there are significant gaps in the information reported from experimental studies. A significant finding of this report is the recommendations for future experimental welding studies as well as improvements that can be made for future modeling efforts.

15. SUBJECT TERMS
Aluminum, SYSWELD, FEA, CWM

16. SECURITY CLASSIFICATION OF: UNCLASSIFIED			17. LIMITATION OF ABSTRACT	18. NUMBER OF PAGES	19a. RESPONSIBLE PERSON
a. REPORT	b. ABSTRACT	c. THIS PAGE			Charles R. Fisher
UNCLASSIFIED	UNCLASSIFIED	UNCLASSIFIED		22	19b. TELEPHONE NUMBER (301) 227-4969

CONTENTS

Page

FIGURES

TABLES

ADMINISTRATIVE INFORMATION

The work described in this report was performed by the Welding, Processing, and Nondestructive Evaluation Branch (Code 611) of the Platform Integrity Department at the Naval Surface Warfare Center, Carderock Division (NSWCCD). The work was funded in FY21-22 by Dr. William Mullins (Code 332) within the Office of Naval Research (ONR).

ACKNOWLEDGEMENTS

The authors would like to thank Dr. Matthew Dantin (NSWCCD Code 611) and the support team at ESI-North America for their technical assistance in the completion of this work.

This page intentionally left blank

EXECUTIVE SUMMARY

The Welding, Processing, and Nondestructive Evaluation (NDE) Branch (Code 611) at the Naval Surface Warfare Center, Carderock Division (NSWCCD) was tasked with developing a digital twin of an experimental welding study to evaluate the residual stress and distortion of aluminum B2V.1 joints. The intent of the study was to validate the computational welding model, developed using a welding-based finite element analysis (FEA) software called SYSWELD, through the comparison of predicted and measured distortion values. However, the previous study that provided the experimental basis of this work did not include all of the information necessary for model validation, and the large number of assumptions made in the model, which resulted in inaccurate predictions. This study provides an example of the limitation of computational modeling when there are significant gaps in the information reported from experimental studies. A significant finding of this report is the recommendations for future experimental welding studies as well as improvements that can be made for future modeling efforts.

BACKGROUND

The Welding, Processing, and Nondestructive Evaluation (NDE) Branch (Code 611) of the Naval Surface Warfare Center, Carderock Division (NSWCCD) was tasked with quantifying differences between recently developed synergic gas metal arc welding (GMAW) processes in comparison to more conventional GMAW techniques. Synergic welding processes are a variant of pulsed GMAW, with unit current pulses to enable detachment of uniform molten droplets. Each synergic process is unique to a given material grade, filler metal, and shielding gas, which yields a complex waveform requiring data collection at high acquisition rates to fully capture the pulse frequency [1]. Synergic processes are distinguished from pulsed GMAW processes by the three following characteristics: 1) automatic selection of pulse parameters, 2) pulse frequency directly related to wire feed rate, and 3) electronic control of welding parameters [2].

This comparison effort involved using various power supplies from Fronius, Lincoln Electric, and Miller to weld aluminum alloy AA 5456-H116 plates together using ER5556 welding wire. All weldments consisted of three to four-passes, single-v-groove welds in a butt joint configuration, corresponding to a B2V.1 joint specified by MIL-STD-22D [3]. The weldments consisted of various combinations of flat, unsensitized plate and sensitized shipboard plate with nominal thicknesses of 9.525 mm (0.375-in.) and 12.7 mm (0.25-in.), respectively. Sensitization is the cumulative exposure of 5XXX-series aluminum to elevated temperatures, causing the magnesium in the alloy to migrate to the grain boundaries which can lead to premature failure [4]. The tasking was to understand the effect of welding older, in-service plate (*i.e.*, representing weld repair) against new plate (*i.e.*, new construction).

In support of the Code 611 welding effort, the Performance Evaluation Branch (Code 653) at NSWCCD measured distortion of the plates throughout the welding process using a Steinbichler Model 5-11M white light measurement system, a non-contact, three-dimensional (3D) survey technique. Code 653's report summarizes the techniques used and the distortion measurements taken for the various welded plate combinations [5]. An offshoot of this effort was

to use the white-light measurements as a verification and validation (V&V) step of weld simulations run by Code 611. The V&V was guided by the computational weld mechanics techniques set forth in the American Welding Society (AWS) A9.5 *Guide for Verification and Validation in Computational Weld Mechanics* (CWM) [6]. This best practices method was used to understand how modification of the thermal input using synergic GMAW processes would affect the resultant distortion predictions using CWM-based methods.

Since 2012, Code 611 has investigated thermal input, distortion, and residual stress evolution in weldments using *SYSWELD*, a commercially available thermo-physical, thermo-mechanical finite element analysis (FEA)-based weld simulation software. The sensitized plate in the synergic welding study was severely deformed, as noted in [5], thus requiring extreme clamping in order to obtain flat surfaces suitable for welding. Therefore, this simulation effort focused on modeling the weld process for unsensitized to unsensitized Al plates only, as these were nominally flat prior to welding.

PROCEDURE

NSWCCD Code 611 engineers used *SYSWELD* software, leveraging FEA and computer-aided design (CAD) techniques, to simulate the fabrication conditions of the B2V.1 joints. For the physical weldments, unsensitized AA 5456-H116 plates were welded with ER5556 welding wire. An AA 5052-H34 database provided by ESI (the developers of the *SYWELD* software) to Code 611 was modified to match the thermo-physical and thermo-mechanical properties of AA 5456-H116 using data previously collected at Alcoa which is now contained within ASM handbooks [7-8]. To assess the impact of material properties on the predicted distortion, simulations were conducted for each weldment using both the original AA 5052-H34 and the modified AA 5456-H116 material databases. **Table 1** shows a comparison between the thermal conductivity, 0.2% offset yield strength, and ultimate tensile strength (UTS) for these three materials at room temperature (20 °C [68 °F]). Temperature-dependent material properties for the ER5556 filler metal were not readily available, therefore base plate material was used in all simulations instead per guidance from AWS A9.5 [6]. It should be noted that the *SYSWELD* software is also able to account for a reduction in thermo-mechanical properties due to welding, namely switching the appropriate elements to material properties associated with AA 5456-O temper.

Table 1. Typical Room Temperature Material Properties for Three Aluminum Alloys

	Thermal Conductivity		0.2% Yield		UTS	
Material	**W/m·K**	**BTU/hr·ft·°F**	**MPa**	**ksi**	**MPa**	**ksi**
AA 5052-H34 [9]	138	79.7	214	31	262	38
AA 5456-H116 [7-8]	125	72.2	255	37	352	51
ER5556 (as welded) [10]	--	--	159	23	310	45

The unsensitized plates were 9.525 mm (0.375-in.) thick, 203.2 mm (8-in.) wide, and either 508 mm (20-in.) or 609.6 mm (24-in.) long. The B2V.1 joint had a 60° included angle (30° bevel on each plate) with a 1.59 mm (1/16-in.) land. **Table 2** details the four different welding techniques used, including pulsed GMAW using a Miller Alumaweld 350 conventional (constant

voltage) GMAW on a Lincoln Electric S500 (Mode 5), and synergic GMAW on either the Lincoln Electric S500 (Mode 157) or a Fronius TransPuls Synergic 2700. **Table 2** also gives the plate sizing and parameters used for each of the four simulations. The shorthand name is used as the naming convention for each weldment for the remainder of the report.

Table 2. Welding Type, Machine, and Plate Sizing for the Various Weld Simulations

			Plate Sizing (mm) [in]		
Weld Type	**Shorthand**	**Machine**	**Thickness**	**Width**	**Length**
Pulsed GMAW	GMAW-P	Miller Alumaweld 350	9.525 [0.375]	203.2 [8]	508 [20]
Conventional GMAW	GMAW-C	Lincoln S500			609.6 [24]
Synergic GMAW	GMAW-S (L)	Lincoln S500			508 [20]
	GMAW-S (F)	Fronius TransPuls Synergic			

CAD Models

The *SYSWELD* software was used to generate three-dimensional (3D) CAD models of each of the four single-v-groove weld scenarios with a representative model shown in **Figure 1**. **Figure 2** shows the cross-sectional weld bead profile of each model with their respective weld bead sizes as estimated from the exterior of the physical welds. Measurements of the external weld bead sizing after fabrication allowed calibration of the CAD model to the physical welds, a technique detailed in AWS A9.5 [6]. However, the size and morphology of the subsurface weld beads was estimated as no weld cross-sectional macrograph was provided. Additionally, the size of the back-gouge region was also assumed based on discussions with NSWCCD welding technicians based on their experience completing similar tasking. As noted in **Figure 2**, in terms of weld bead size, relatively minor changes (less than 5 mm [0.20-in.]) were noted across the four different welding scenarios. The average element side length in the through-thickness area near the weld passes was set to 1 mm (0.04-in.), whereas along the weld path, an element side length of 3 mm (0.12-in.) was used in order to reduce the simulation completion time.

Figure 1. Representative CAD model showing the B2V.1 joint configuration. The red box (left side) shows the magnified cross-sectional view shown in **Figure 2**.

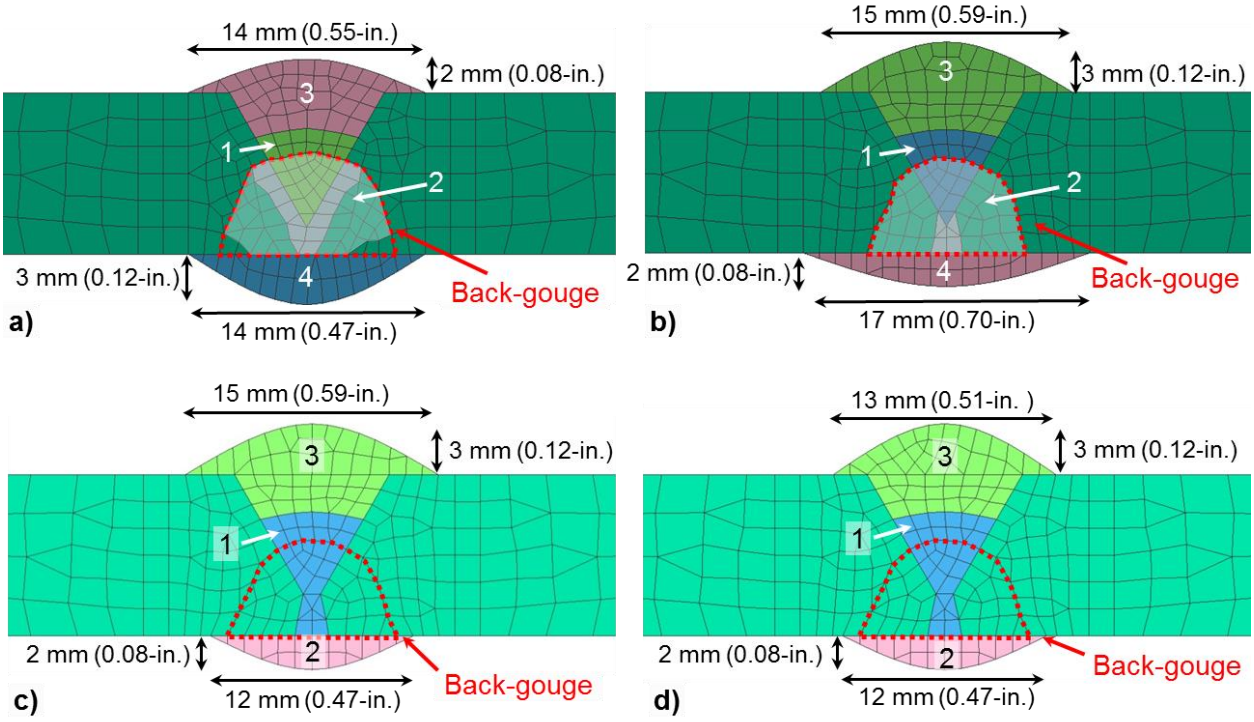

Figure 2. *SYSWELD* CAD models with cover pass bead sizing illustrating the mesh near the welded zone for the **a)** GMAW-P, **b)** GMAW-C, **c)** GMAW-S (L), and **d)** GMAW-S (F) weld scenarios. Notice the back-gouge areas displayed by the red-dotted shape. The single digits represent the number of each respective weld pass. In **a)** and **b)**, the white transparent area represents the area of the third welding pass (not found in the synergic welding scenarios).

As shown in **Figure 2**, welds made with GMAW-P and GMAW-C had four weld passes, whereas the two synergic weldments had only three passes. For the GMAW-P and GMAW-C welds, the fabrication process initiated by welding the root of the bevel (#1), flipping the weldment, back-gouging along the length of the weld, welding the back-side root pass (#2), flipping the weldment a second time, completing the front-side cover pass (#3), flipping the weldment a third time, and completing the back-side cover pass (#4) as shown in **Figure 2a-b**. For the GMAW-S (L) and GMAW-S (F) welds, the fabrication process initiated by welding the root of the bevel (#1), flipping the weldment, back-gouging along the length of the weld, welding the back-side cover pass (#2), flipping the weldment a second time, and completing the front-side cover pass (#3) as shown in **Figure 2c-d**. Although not reported in the welding procedure for any of the four weld scenarios, it was assumed that the physical clamps are removed and reapplied between each flip of the plate after the weld was cooled to ambient temperature.

The NSWCCD welder completing the fabrication noted that the GMAW-P, GMAW-C, and GMAW-S (F) each had repairs made for non-conforming weld passes. However, except for the GMAW-C scenario, these were not simulated due to lack of precise repair information (*i.e.*, position, gouge depth and length, repair weld bead size, and other essential weld parameters). For the GMAW-C repair, sufficient detail was provided to simulate the repair process. Therefore, for the GMAW-C simulation, the first three weld passes were completed as normal. A second gouge step removed all elements associated with the #3 weld pass and another weld pass was initiated (Weld #3A). Then a third gouge step removed the first 114.3 mm (4.5-in.) elements of Weld #3A and a repair weld pass was initiated to fill in this volume (Weld #3R). In this way, the entire thermal load from each weld pass and repair was able to be simulated.

The gouge areas shown in **Figure 2** and described above for the repairs in the GMAW-C scenario are simulated by removing the elements in the gouged area. As recommended by ESI, the gouge process was initiated by deactivating the original elements for the remainder of the simulation. Then a set of new elements are added, which are coincident with the original gouge, representing the filler wire being deposited. Although the elements are coincident, it was recommended that the nodes in the area to be fused together to account for any distortion prior to gouging. This allows for more precise mechanical calculations during simulated material removal steps and is referred to as the element “birth-and-death” method [11].

As illustrated in **Figure 2**, the deposited area of each weld was simulated as filler material as opposed to plate material. Although the fluid flow of the weld pool is not included in the *SYSWELD* model, each weld pass is given a so-called “chewing gum”-type consistency within *SYSWELD* (a standard practice within the software) to maintain a connected mesh. This technique does not increase the stiffness of the system during mechanical simulation while the specific element is simulated to be at a temperature above the solidus. After cooling from the molten state, *SYSWELD* uses the defined thermal, mechanical, and metallurgical material properties of the simulated material. In this way, the connected mesh in the weld bead area does not interfere with the mechanical calculations until after the weld has solidified. This imitates reality during the first weld pass, as the two plates are not “connected” while the weld is in the molten state. Upon subsequent weld passes, the now-solidified weld zone does tend to increase the overall stiffness of the weldment structure.

To assess the influence of the material database on the predicted distortion, three simulation conditions were used for the *SYSWELD* models in **Figure 2**. The first condition designated as “5052 Database” utilized the AA 5052-H34 database that was provided by ESI [9]. For this model, the thermal cross-section of each weld was optimized by modifying the heat source conditions (weld efficiency, penetration, length and width). The second test condition designated as “5456 with 5052 Thermal Database” (5456_5052) utilized identical heat source parameters as the first condition with a user-defined AA 5456-H116 database, which included the AA 5456-H116 material properties from Alcoa [7-8]. The third simulation condition designated as “5456 Database”, utilized the same user-defined AA 5456-H116 material database, but with the optimized heat source conditions for that database. As the plate material was AA 5456-H116 for the physical experiments, the 5052 Database condition describes the influence of an incorrect material database, the 5456_5052 describes the use of improper heat source parameters and the 5456 Database condition describes the ideal scenario with the correct heat source conditions and material data.

The clamping conditions for the four weld simulations is displayed in **Figure 3** with two types of clamps defined in the simulations. The first type of clamping used are the elastic clamps along the length of the weld plates. These clamps represent physical clamps used to hold the plates in place during the welding process. Starting at approximately 25.4 mm (1-in.) from the plate edges, elastic clamps were placed along the length of the plate on each side of the weld line. Seven clamps were used for the 508 mm (20-in.) long models [GMAW-P, GMAW-S (L), and GMAW-S (L)] and nine clamps for the 609.6 mm (24-in.) long model [GMAW-C]. Each elastic clamp consisted of the four nodes around the elements highlighted in yellow. The elastic clamps had an elastic stiffness of 10,000 Pa (1.45 psi) in-plane and 100 Pa (0.0145 psi) perpendicular to the plane. Each model exhibited an identical set of clamps on the backside of the plates, which were used to simulate the flipping of the plate through deactivating one side and activating the other side.

The second type of clamping condition is referred to as “unclamping”, indicated by the red stars in **Figure 3**. These nodes were activated with the simultaneous deactivation of the elastic clamps for the final 500 second cooling period at the end of each simulation. Therefore, the model accounts for the release of the elastic clamps, resulting in stress relaxation and part distortion. The unclamping approach is recommended over the use of rigid clamps in the weld bead area as the models with the rigid clamps resulted in severe distortion of the elements that was not representative of reality.

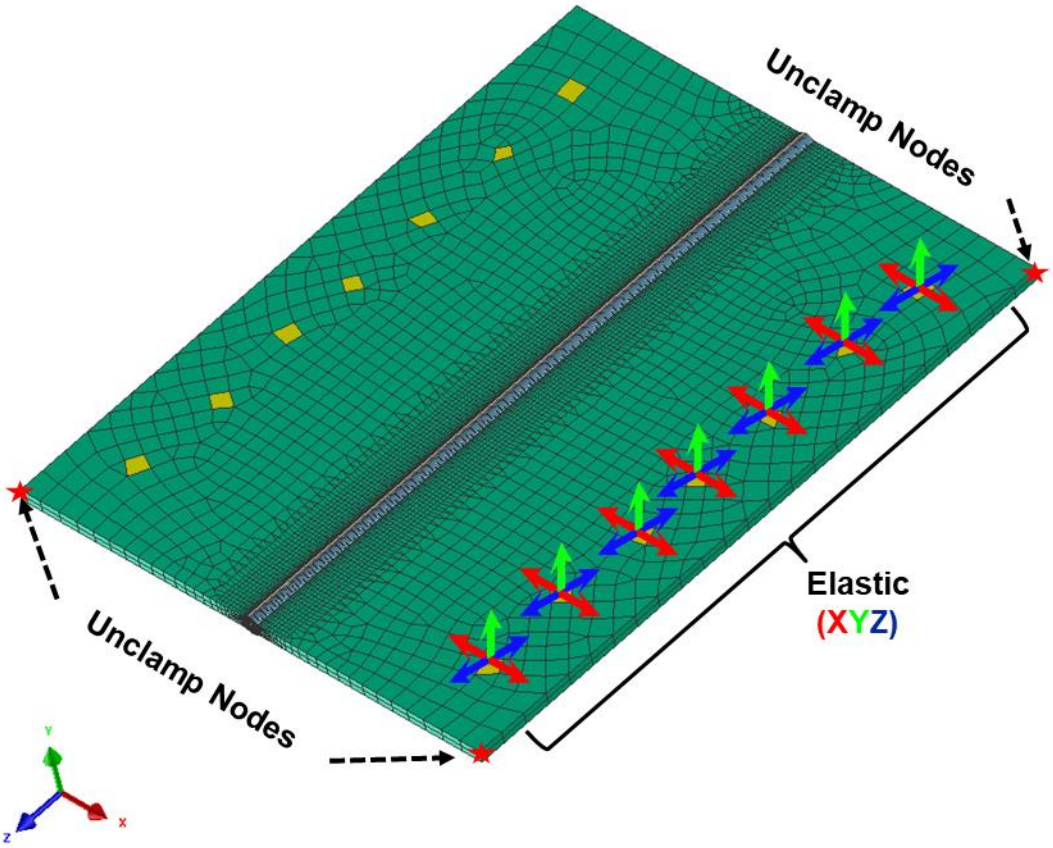

Figure 3. Representative meshed CAD model displaying the location of the unclamp nodes at the corner of each plate and the elastic clamps along the top of the GMAW-S (F) model with clamps on the other half of each model in mirror positions (yellow quadrangles). These clamps are analogous to clamp positions for GMAW-P and GMAW-S (L) models. For the GMAW-C, the clamp positions are similar but with an extra two clamps on each side along the length of the weld as it is 609.6 mm (24-in.) long instead of only 508 mm (20-in.).

Weld Process Simulation Parameters

Simulations were set-up on *Visual Environment* (version 16.0.1) and run using the *SYSWELD* solver (version 2020.0). A 3D, transient heat source process simulation using a Goldak heat source model [12] was used to compare the different GMAW scenarios. The weld process parameters replicated those from the actual welding procedure for each of the four scenarios.

The welding parameters for each weld pass of each welding scenario are found in **Table 3** and **Table 4**. For a conventional GMAW process, an average welding arc efficiency has been measured to be 85% ± 4% [13], which served as the basis for the initial parameter analysis for preliminary 2D and 3D simulations. Only the final 3D thermomechanical simulation parameters are recorded in this report. The arc efficiency as well as the input bead size dimensions were modified to determine optimized conditions for the AA 5052-H34 database and AA 5456-H116

modified database with the optimized AA 5052-H34 thermal conditions listed in **Table 3**. These parameters were adjusted to optimize the weld bead thermal profile for the AA 5456-H116 modified database as shown in **Table 4**.

Table 3. Welding Parameters Used for the 5052 and 5456_5052 Database Simulations

Scenario	Weld Pass	Arc Eff. (%)	Travel Speed (mm/s) [in/min]	Heat Input (J/mm) [kJ/in]	Bead Size (mm) [in]		
					Length	Width	Penetration
GMAW-P	1	97	7.41 [17.5]	404.8 [10.3]	10 [0.39]	7 [0.28]	7 [0.28]
	2	87	5.21 [12.3]	621.9 [15.8]	8 [0.31]	12 [0.47]	3 [0.12]
	3	85	4.49 [10.6]	846.1 [21.5]	10 [0.39]	10 [0.39]	3 [0.12]
	4	100	4.02 [9.5]	806.0 [20.4]	9 [0.35]	12 [0.47]	2 [0.08]
GMAW-C	1	82	4.45 [10.5]	707.8 [17.9]	10 [0.39]	8 [0.31]	3 [0.12]
	2	71	2.62 [6.2]	1350.4 [34.2]	9 [0.35]	8 [0.31]	4 [0.16]
	3	91	3.13 [7.4]	1052.4 [26.7]	9 [0.35]	10 [0.39]	4 [0.16]
	3A	95	4.36 [10.3]	853.9 [21.7]	9 [0.35]	9 [0.35]	3 [0.12]
	3R	85	4.02 [9.5]	1062.7 [26.9]		9 [0.35]	
	4	85	3.26 [7.7]	1253.1 [31.8]		10 [0.39]	
GMAW-S (L)	1	90	6.69 [15.8]	479.1 [12.1]	6 [0.24]	6 [0.24]	3 [0.12]
	2	92	4.83 [11.4]	676.4 [17.1]			
	3	98	3.89 [9.2]	863.9 [21.9]		8 [0.31]	
GMAW-S (F)	1	90	6.99 [16.5]	483.1 [12.4]	6 [0.24]	6 [0.24]	3 [0.12]
	2	97	3.98 [9.4]	697.1 [17.7]		8 [0.31]	4 [0.16]
	3	100	2.54 [6.0]	956.6 [24.2]		10 [0.39]	3 [0.12]

Table 4. Welding Parameters for the 5456 Database Simulations

Scenario	Weld Pass	Arc Eff. (%)	Travel Speed (mm/s) [in/min]	Heat Input (J/mm) [kJ/in]	Bead Size (mm) [in]		
					Length	Width	Penetration
GMAW-P	1	88	7.41 [17.5]	404.8 [10.3]	10 [0.39]	7 [0.28]	6 [0.24]
	2	82	5.21 [12.3]	621.9 [15.8]	10 [0.39]	13 [0.51]	1.8 [0.07]
	3	74	4.49 [10.6]	846.1 [21.5]	10 [0.39]	13 [0.51]	2 [0.08]
	4	85	4.02 [9.5]	806.0 [20.4]	10 [0.39]	13 [0.51]	2 [0.08]
GMAW-C	1	75	4.45 [10.5]	707.8 [17.9]	10 [0.39]	8 [0.31]	3 [0.12]
	2	65	2.62 [6.2]	1350.4 [34.2]	9 [0.35]	8 [0.31]	3 [0.12]
	3	82	3.13 [7.4]	1052.4 [26.7]	9 [0.35]	10 [0.39]	4 [0.16]
	3A	80	4.36 [10.3]	853.9 [21.7]	9 [0.35]	9 [0.35]	3 [0.12]
	3R	72	4.02 [9.5]	1062.7 [26.9]		9 [0.35]	
	4	73	3.26 [7.7]	1253.1 [31.8]		10 [0.39]	
GMAW-S (L)	1	82	6.69 [15.8]	479.1 [12.1]	6 [0.24]	6 [0.24]	3 [0.12]
	2	78	4.83 [11.4]	676.4 [17.1]		6 [0.24]	
	3	84	3.89 [9.2]	863.9 [21.9]		8 [0.31]	
GMAW-S (F)	1	80	6.99 [16.5]	483.1 [12.4]	6 [0.24]	6 [0.24]	3 [0.12]
	2	85	3.98 [9.4]	697.1 [17.7]		8 [0.31]	4 [0.16]
	3	90	2.54 [6.0]	956.6 [24.2]		10 [0.39]	3 [0.12]

For all of the simulations, the starting temperatures were set at 20 °C (68 °F). The inputted time between the weld passes was 1000 seconds, allowing each weldment to drop below the specified interpass temperature of 65 °C (150 °F) prior to the initiation of the following pass. Every weld pass used *SYSWELD* default parameters for Length Ratio (1.2) and Power Ratio (0.5) of the Goldak heat source model [12]. **Table 5** shows the energy ramp for each weld pass, used to simulate conditions at the beginning and termination of each weld path.

To simulate the cooling post-weld of each model, a 2D boundary condition was constructed around the surface area of the final model. The radiative and convective losses at this

boundary were simulated using a radiation emissivity (ε_0) of 0.8 and convective heat transfer coefficient (h_c) of 25 W/m^2/K. These are the set values within the *SYSWELD* software for a "free air cooling" scenario. This boundary condition was utilized throughout the entire welding process, and enabled radiative and convective transfer through the external surfaces while the ambient temperature was kept at 20 °C (68 °F). In order to simplify the model complexity and reduce computational time, the conductive heat transfer of the plate to the worktable was not simulated.

Table 5. Energy Ramp Weld Parameters for the SYSWELD Simulations

		Beginning of Weld		Termination of Weld	
Scenario	**Weld**	**Length (mm) [in]**	**Energy Factor**	**Length (mm) [in]**	**Energy Factor**
GMAW-P	1	10 [0.39]	1.5	10 [0.39]	0.75
	2				
	3	8 [0.31]		8 [0.31]	
	4	10 [0.39]		10 [0.39]	
GMAW-C	1	10 [0.39]	1.5	15 [0.59]	0.3
	2	9 [0.35]		12 [0.47]	
	3			9 [0.35]	
	3A				
	3R				0.75
	4			18 [0.71]	0.3
GMAW-S (L)	1-3	6 [0.24]	1.5	12	0.1
GMAW-S (F)	1-3	6 [0.24]	1.5	12	0.1

RESULTS AND DISCUSSION

The *SYSWELD* models were evaluated to determine the evolution of distortion produced by the welding process. Unless otherwise noted, the reported distortion represents the completed welding process, after the final unclamping step and cooling back to room temperature.

Influence of Welding Thermal Input Parameters

The thermal profiles in **Figure 4** shows a cross-section at the mid-point of the weld, illustrating the maximum temperature predicted throughout the entire simulation. The pink color represents the area of each model predicted to exceed 600 ºC (1112 ºF), the approximate solidus of aluminum 5XXX series alloys [14]. This technique follows AWS A9.5 [6] for V&V of CWM-based weld simulations. As shown, all weld passes realized full melting during welding, which ensures greater accuracy of the shrinkage forces realized by cooling to room temperature (and thus welding-induced distortion).

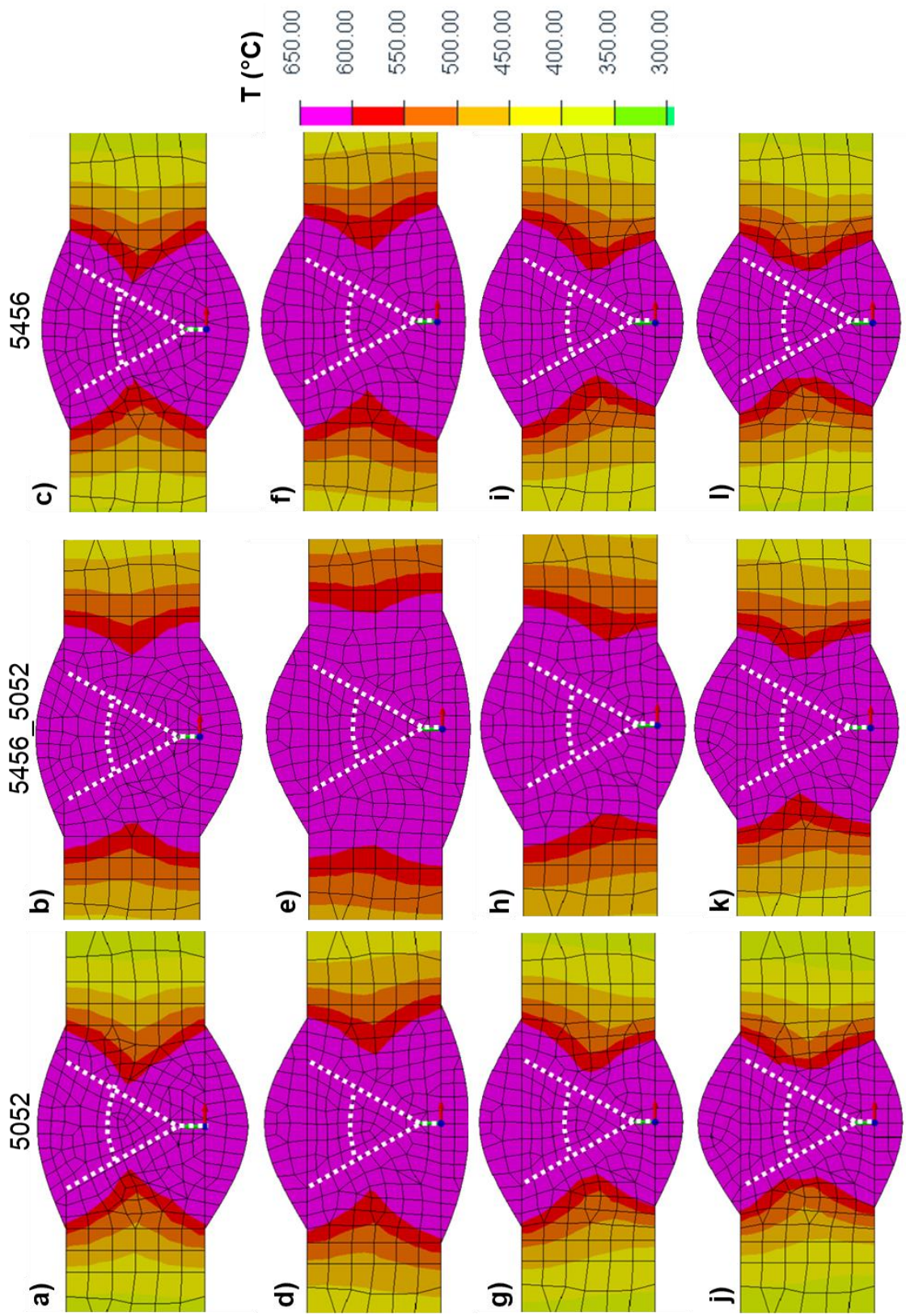

Figure 4. Cross-section at the mid-point of the weld length illustrating the maximum temperature prediction in the weld area from *SYSWELD* simulations for the **a-c)** GMAW-P, **d-f)** GMAW-C, **g-i)** GMAW-S (L), and **j-l)** GMAW-S (F) weld scenarios. Each column indicates the database and thermal conditions used as described by the database conditions: 5052, 5456 with 5052 thermal optimization and 5456. The pink area (T > 600 °C [1112 °F]) represents the area that is predicted to melt during the welding process. The white, dashed lines represent the original single-v-groove plate configuration.

As described by **Table 3**, the 5052 and 5456_5052 conditions used the same heat source parameters. However, this resulted in significant over melting of the base plate material for the 5456_5052 condition. This is likely caused by the difference in thermal conductivity as shown in **Figure 5**, where there is a significant difference in thermal conductivity for the two aluminum alloys below 400 °C (752 ºF).

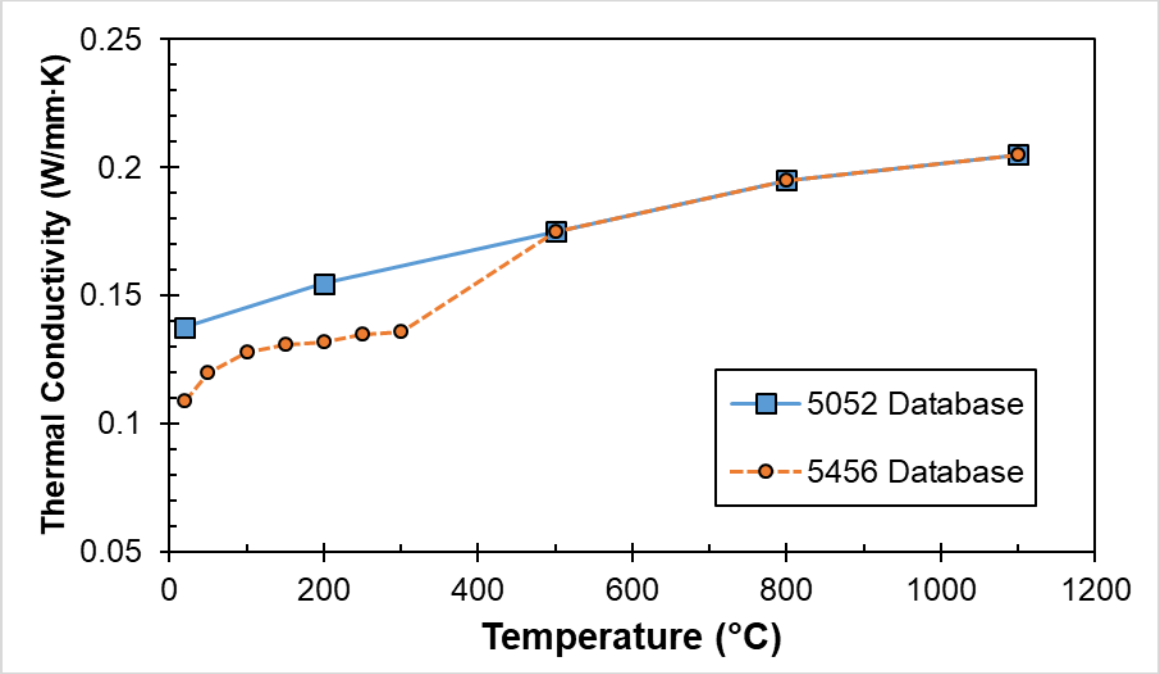

Figure 5. Comparison of the temperature-dependent thermal conductivity for the 5052 and 5456 material database.

As the heat input and travel speed were fixed parameters for each weldment, the arc efficiency and Goldak heat source parameter were adjusted between the 5052 and 5456 databases to achieve an optimized thermal profile where the entire weld bead area is molten (>600 °C [1112 °F]). This resulted in a correction in the over melting of the weld bead area, as indicated by the comparison of the 5456_5052 cross-sections to the 5456 cross-sections in **Figure 4.** In this study, the bead size was approximated for each weldment as a weld cross-section was not provided. However, under ideal circumstances, the width and penetration should be given values that are experimentally measured by macro cross-section image analysis.

The different arc efficiencies were likely due to the difference in thermal properties of AA 5052-H34 and AA 5456-H116, as a consistent reduction in arc efficiency was required to correct for the over melting shown in the 5456_5052 models. This indicates that with differences in material thermal properties, adjustments must be made to the model to represent realistic welding conditions.

Nodal Distortion

The white-light measurement technique yielded a point cloud with ~11,000,000 points for each step. **Figure 6** shows example datasets of each scenario from the data processing. The

measurement and post-processing of the data is fully described in reference [5]. For the CWM-based FEA simulations, the distortion was measured by displacement of any single node within the 3D mesh compared to that node's original position. To compare between the FEA and white-light data, the distortion was calculated as the difference in position from the initial plate elevation to the post-weld elevation.

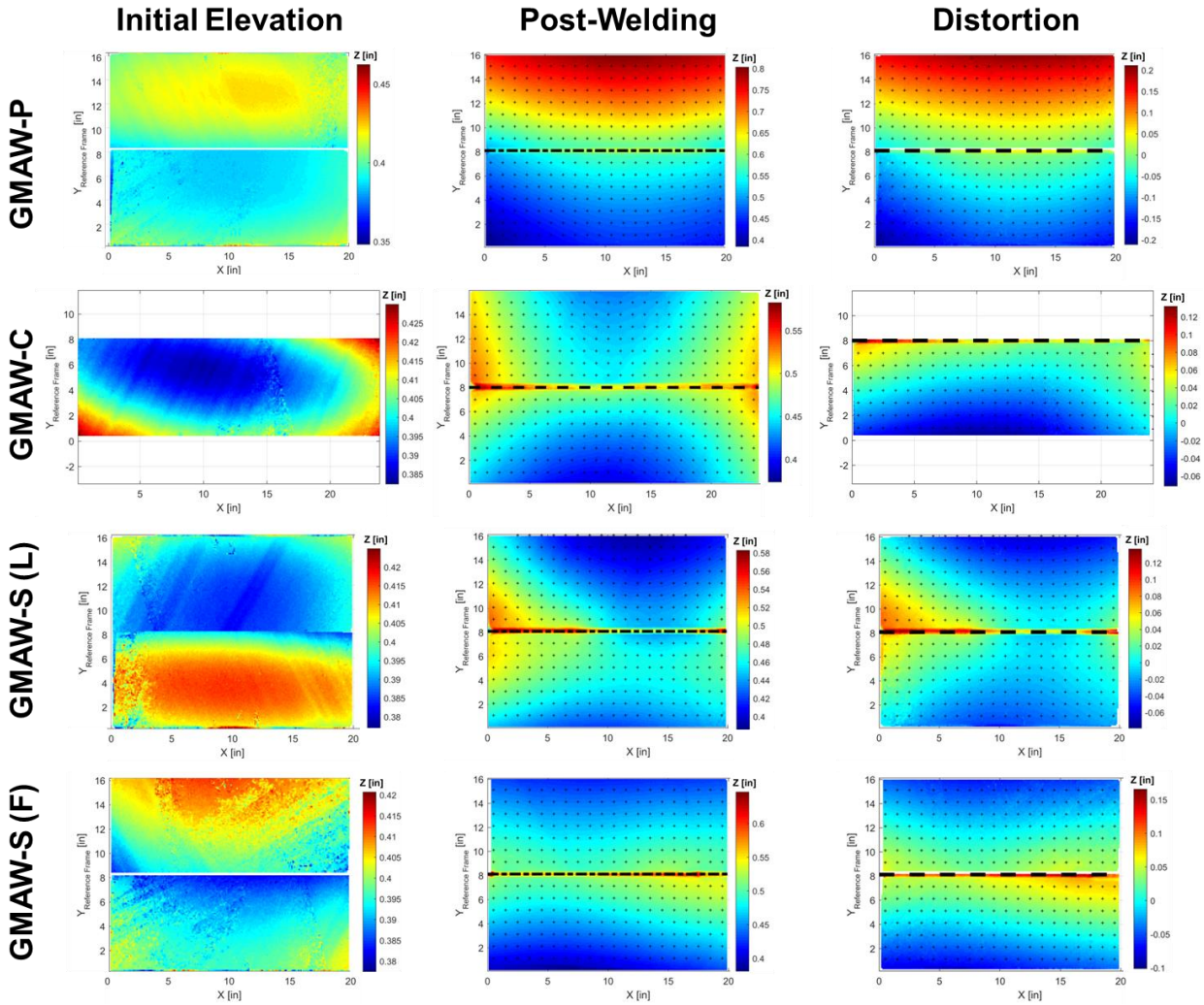

Figure 6. Example elevation charts displaying the white light measurement data for each of the B2V.1 weld scenarios representing the initial plate, post-welding, and distortion states. The black dashed lines represent the weld path and each black dot represents a point in the data grid utilized for comparison to the FEA simulations. Note that some of the pre-weld data for GMAW-C scenario was not available, thus a lack of distortion data from one of the plates. Data adapted from reference [5].

Figure 7a-l shows a comparison of the final distortion state for the four simulated welds and three database conditions with the original position of the plate shown in teal. The color represents the distortion predicted by *SYSWELD* after the final unclamping step, where the plate distorts to partially relieve residual stress. It was noted that the magnitude of the final distortion

is less sensitive to changes in the material database utilized and more sensitive to the changes in welding parameters and weld sequence. For example, the four-pass GMAW-P and GMAW-C models yield an angle bend opposite the three-pass synergic GMAW-S [L] and GMAW-S [F] models (V-shape vs. Λ-shape). This is due to the final weld pass being on the backside of the plate for these conditions when compared to the synergic welds, where the final pass is on the top of the plate. However, the orientation of the distortion for the synergic welds changes from a negative displacement to a positive displacement with the use of the AA 5456-H116 modified database. Further analysis is needed to determine why this occurred.

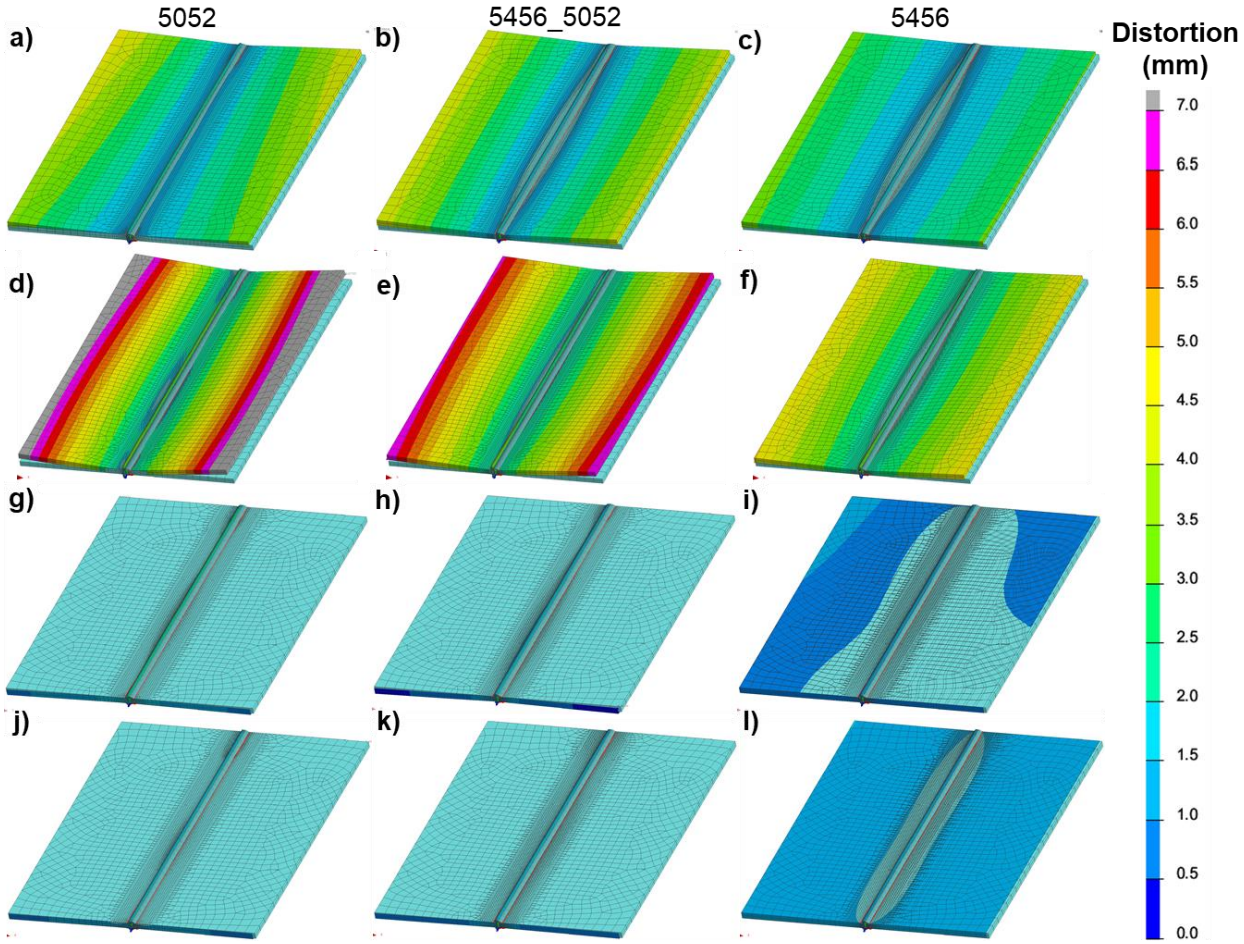

Figure 7. *SYSWELD*-generated distortion predictions [amplified by three times for ease of visibility] for the **a-c)** GMAW-P, **d-f)** GMAW-C, **g-i)** GMAW-S (L), and **j-l)** GMAW-S (F) weld scenarios. Each column indicates the database and thermal conditions used as described by the database conditions: 5052, 5456 with 5052 thermal optimization, and 5456.

Due to the vast number of data points generated by the white light measurements six representative data points were selected as comparison points across the four weld scenarios. **Figure 8** shows the location of the six points selected for the nodal distortion comparison, taken from the final step of the *SYSWELD* simulations. **Figure 9a-d** shows comparison plots of the

measured white light measurements and the predicted *SYSWELD* distortion for each welding and material database condition.

As indicated by the comparison of the *SYSWELD* predicted distortion to the distortion measured by the white light measurements, the models exhibited sufficient agreement with the measured values with the exception of the GMAW-C condition. Unlike the other weld scenarios, the GMAW-C condition was much more complex as it consisted of a total of six welds and three gouge steps (**Table 3**). As welded cross-sections were not available to validate the size of the weld bead area, it is likely that the assumption of weld bead size led to significant error as well as the lack of specific information about the gouging steps. In *SYSWELD*, gouge steps are conducted by deactivating the elements in the gouged region. This allows the stress to be redistributed to the elements which were not removed and is therefore highly dependent on the volume of material removed. This volume was estimated for each weld as measurements were not included in the previous report [5], which likely contributed significant error in the mechanical modeling of this scenario. This may explain why the predicted distortion for the highly gouged model (GMAW-C) was significantly different from the measured values. Additionally, the GMAW-C scenario may have had the clamps removed after each step and after each gouging step (thought this was not noted in reference [5]), which may have flattened the plate out even more.

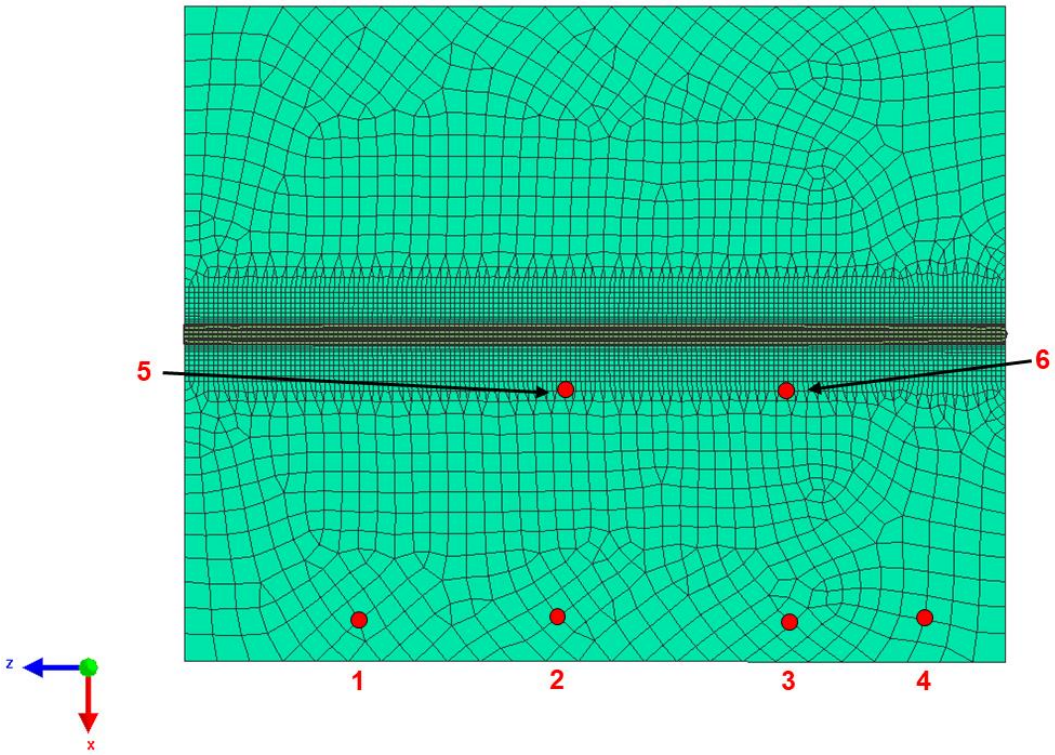

Figure 8. Nodes selected for comparing the *SYSWELD* predicted distortion of the final step of the simulation to the white light measurements. Points 1-4 represent distortion near the edge of the plate and points 5-6 represent the distortion near the weld bead area.

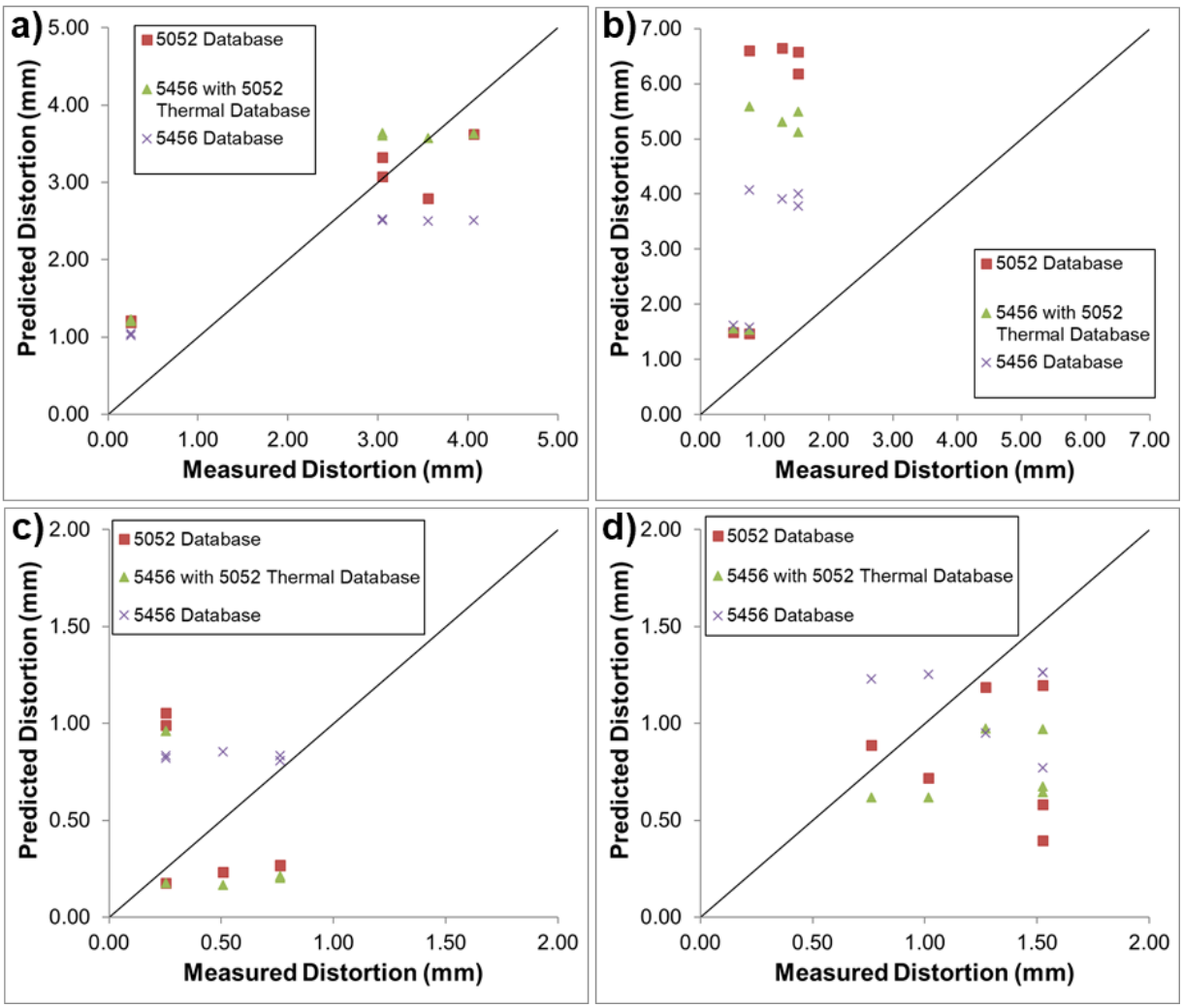

Figure 9. Comparison of the predicted distortion to the white light measurements for the three material database conditions with the **a)** GMAW-P, **b)** GMAW-C, **c)** GMAW-S (L), and **d)** GMAW-S (F) weld scenarios.

Influence of Material Database on the Weld Distortion

Although the simulations using the 5456_5052 condition exhibited an incorrect thermal profile, resulting in over-melting of the weld region (**Figure 4**), there was no significant difference in the predicted distortion in the nodes near the weld region (**Figure 9**). This is consistent for the nodes at the edge of the plate for all conditions with the exception of the GMAW-C condition, where there appears to be an improvement in the predicted distortion when compared to the 5052 database condition. These results suggest that the predicted distortions are not sensitive to having an optimized thermal profile in the weld bead area, which is surprising since it goes against current best practices (see AWS A9.5 [6]). Therefore, it is believed to be a convolution of factors associated with the modeling inputs (both material and process) resulting in the obvious over-melting (which would not be realistic to achieve a good weld in reality) and

thus the atypical mechanical response. The authors are not suggesting that future weld modeling efforts need not focus on proper bead sizing.

The difference in the mechanical properties between the AA 5052-H34 and AA 5456-H116 modified databases is shown in **Figure 10**. As the physical welds were conducted with AA 5456-H116 plates, it would be expected that the use of the correct material database will improve the simulation accuracy when using the optimized thermal profile. However, there is no clear improvement in accuracy of the predicted distortion with the use of the AA 5456-H116 modified database. This suggests there are other factors not being included in the model.

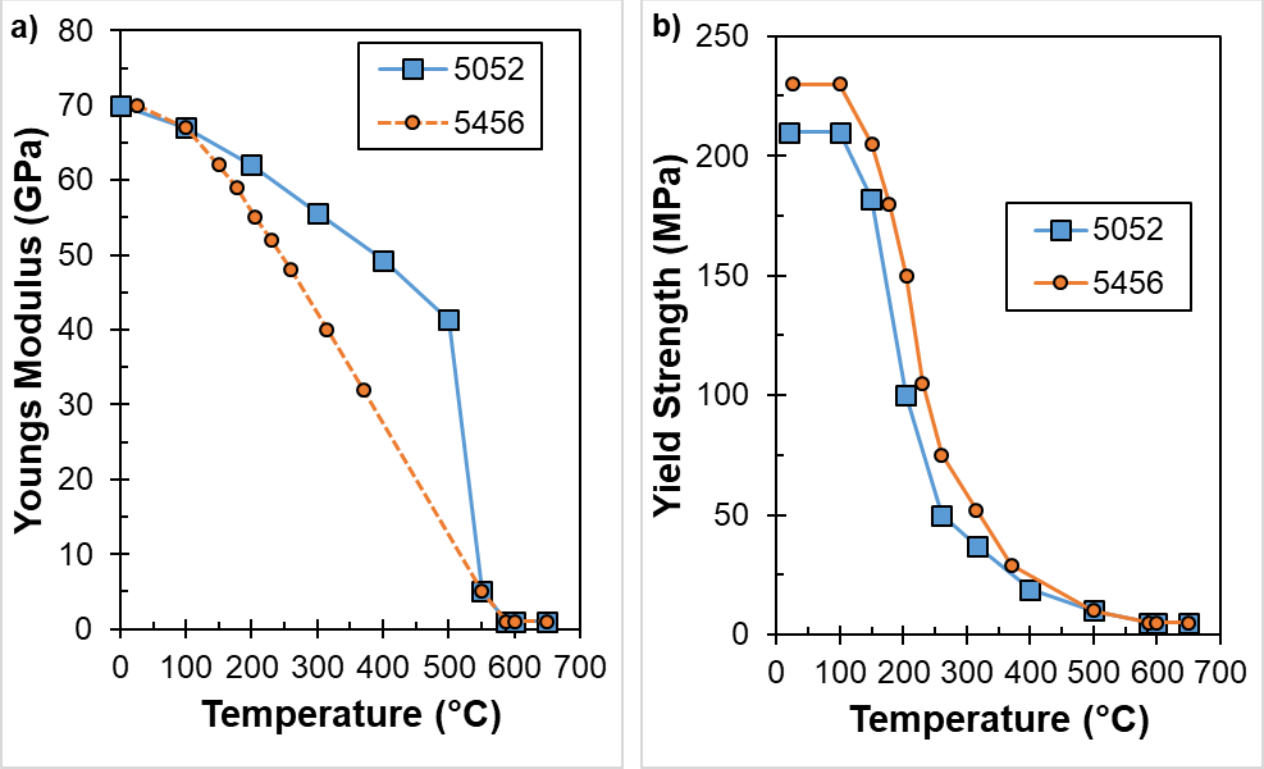

Figure 10. Mechanical property comparison of the **a)** Young's modulus and **b)** yield strength as a function of temperature for the Al 5052 and Al 5456 databases.

As a metric of comparison, the absolute value of the percent error was calculated for the six points comparing the predicted and measured distortion for each test case. These values were then averaged to provide the calculated error for each test condition as shown in **Table 6**, where due to the large standard deviation of each case, there is no statistically significant difference in the prediction accuracy of the different material database conditions. This suggests that the material database selection only imposed minor differences in predicted distortion, again suggesting there were additional factors not being included in the simulations.

This observation regarding the simulation results could also indicate that having a representative material database within a particular class (*i.e.*, a general 5XXX aluminum alloy database instead of AA 5052-H34) is most important. However, this observation goes against

current best practices within the CWM industry, and thus requires further work before final conclusions can be drawn.

Table 6. Comparison of Distortion for Simulated and Physical Weld Scenarios

	Percent Error ± 1σ		
Scenario	**5052**	**5456_5052**	**5456**
GMAW-P	132 ± 188	135 ± 190	120 ± 146
GMAW-C	352 ± 233	293 ± 181	214 ± 115
GMAW-S (L)	136 ± 129	133 ± 113	127 ± 107
GMAW-S (F)	35 ± 27	38 ± 16	32 ± 19

Distortion Experiment Best Practices

As discussed previously, the simulation results presented do not provide an accurate representation of the physical system when compared side-by-side. This is primarily due to the lack of information provided by the previous study [5] to enable representative modeling of the physical system.

The previous study excluded several key parameters necessary for the development of high fidelity computational simulations. For example, the report did not include the orientation of the plate compared to the reference plane of the distortion measurement, which would change the reference plane of the simulation relative to the distortion measurements. Additionally, it is unknown what (if any) types and sizes of blocks or shims were used to hold the weldment above the table due to the convex root surface extending beyond the plane of the plate edges. As distortion is measured as a relative distance, an accurate simulation of the welding process requires knowledge of where each point was taken on the plate and how the plate is balanced on the surface (especially if it is not flat). Or, in the worst case scenario, if the plate was distorted by dogs, strongbacks, or wedges to clamp the weldment into position despite the convex root surface.

Reference [6] represents an excellent example of a controlled procedure for measuring (and documenting) plate distortion for comparison to computational simulations. To assist in the data acquisition for future reports and to ensure that all the data are reported, a more detailed description of the required parameters was recently completed at NSWCCD in reference [15]. The following subsections briefly describe some of the lessons learned and provide a guide for future welding distortion measurement efforts.

Gouging

If there are obvious defects in the weld warranting removal, the gouging process needs to be documented with images before and after gouging. An inspection sheet with measurements would also be sufficient. Additionally, the type of tool used and (at minimum) approximate dimensions of the volume of removed material is desired. Measured information such as gouge depth and length, bevel angel, and radius of bottom contour would be especially beneficial. For

studies evaluating the distortion involving gouging, a measurement of the weldment distortion in the weld bead area would be insightful.

Clamping

Previous research has indicated that the influence of clamping force and position has a significant impact on the residual stress and plate distortion. If the clamps are positioned closer to the weld bead area, there is likely to be less distortion after welding and a higher concentration of tensile residual stress in the fusion zone. Therefore, reporting the position of the clamps, the size of clamps used, and the order of which they are applied and removed are critical for accurate CWM distortion modeling. Information such as the time at which the clamp is applied and removed is also important to note. If the clamps are removed while the weldment is still hot, there could be a difference in the resulting distortion.

Welding Conditions Dimensions

Macrographs of the weld bead cross-sections are also an important experimental result to report as this provides measurements of the height and width of the weld pool as well as the extent of dilution in the case of dissimilar metal welding. In an ideal case, the experimental study will include *in-situ* measurements of the melt pool during welding to extract an average melt pool length such as the melt pool camera development by NSWCCD engineers (team led by Mr. Matthew Sinfield, Code 611). Additionally, for multi-pass welding conditions, a diagram of the weld bead deposition order and dwell time between passes should be reported. Precise recordings of interpass temperatures and times are needed for each weld in addition to the description of weld preheating conditions. From a modeling perspective it is important to note how the interpass temperature was measured (*i.e.*, at a particular location in or near the weld or a general measurement) or if there was a variation in time between each weld pass.

Simulation Best Practices

During the process of conducting this research, significant observations were made through discussions with experienced FEA modelers and *SYSWELD* training provided by ESI that can be applied to future research. The following subsections briefly describe some of the lessons learned and provide a guide for future modeling efforts.

Meshing

Although tetra elements are easier to mesh with and provide reasonable results for thermal modeling, hex elements are better for modeling stress and distortion as the tetra elements can impose an artificial rigidity. Additionally, when evaluating the distortion of a plate, having the plate partitioned to at minimum four layers of hex elements will increase the accuracy of the simulation and prevent additional mathematical restraint.

Boundary Conditions

For thermal and mechanical modeling, the boundary conditions have a significant influence on the model result. For example, in this study, the welds were made on a working table, which may allow for heat transfer into the workpiece, and should be included as a

boundary condition. While the *SYSWELD* software does incorporate conductive and radiative heat transfer through air cooling, the effect of ventilation (especially if a fan is used for cooling) and convective heat transfer should also be accounted for.

Clamping

Previous studies have indicated that the defined position and parameters of the clamping conditions are the primary driver for changes in plate distortion, even more so than the layer deposition order in multi-pass welding. In many FEA models, there is elastic clamping (where a particular stiffness is defined at each node) and rigid clamping (where the node is unable to move while the clamp is imposed). Elastic clamps are more representative of reality as there will always be a compliance in the clamp material and the stiffness will be much higher in the clamping direction compared to the directions perpendicular to the clamping force, which are only affected by friction. However, in *SYSWELD* the clamps are specified by a particular stiffness (not a pressure), and the number of nodes selected controls the force applied by the clamping condition. Therefore, a sufficient number of nodes should be selected that are representative of the contact area of the physical clamp. Additionally, the exact position and types of clamps used are critical for accurate modeling of the residual stress and distortion. Rigid clamps should not be applied to the weld region, as this results in artificial stress concentrations and warped elements.

When clamps are removed, it is recommended that the unclamping step is applied with the simultaneous deactivation of the rigid/elastic clamps. In *SYSWELD*, this mathematical unclamping removes the free body motion of the system, preventing the weldment from having a simulated “spring” effect after the clamps are released.

Weld modeling

The CWM modeling in *SYSWELD* is phenomenological, where the heat source parameters must be adjusted to sufficiently melt the area of the weld bead cross-section. When a macrograph is available, the width of the melt pool and the penetration should be treated as fixed values. When using the Goldak (double ellipsoid) heat source, the main parameters to be adjusted are the length of the weld pool (this may be able to be measured by in-situ melt pool monitoring), as well as the Length Ratio (1.2 by default) and the Power Ratio (0.5 by default). The welding parameters (heat input, travel speed, *etc.*) should be kept consistent with those of the physical welds. Lastly, although the efficiency for a particular process is not typically known, it should be kept in realistic bounds found in previous studies (*i.e.*, ~ 85% ± 4% for GMAW [13]).

Gouging

For simulating a gouging step in *SYSWELD*, the elements of the gouged region need to be defined as “machined” components with at least one time-step before the next weld is started. This allows for the mechanical model to redistribute the residual stress in the un-gouged region, emulating the physical system. This may result in local distortion associated with the reduced constraint which is why the nodes of the weld metal that fills in the gouged region should be coincident and fused with the gouge itself. However, the elements of the newly deposited weld

metal should only be coincident and not fused, otherwise the model will be prevented from depositing any more material in the same region.

CONCLUSIONS

The *SYSWELD* simulations conducted to predict the distortion of the new, unsensitized Al plate weldments discussed in this report were not accurate when compared to the white light measurements, which served as the experimental validation [5]. This is likely due to the lack of experimental data required to precisely simulate the physical test conditions. To ensure the development of high-fidelity simulations and validation studies in the future, summary recommendations have been provided for experimental and modeling methods.

The results of this study show minor changes in arc efficiency between the welding conditions under the same material database conditions. However, a higher-fidelity comparison would need weld cross-sections, which were not reported in the experimental study that provided the basis of this work. Due to the difference in thermal conductivity between AA 5456-H116 and AA 5052-H34, the arc efficiency and weld pool dimensions needed to be adapted to compensate for over-melting of the 5456_5052 condition. Even with the incorrect thermal profile of the 5456_5052 condition, there was no significant difference in the predicted distortion, a surprising result. This study provides an example of how reliant CWM models are on having the correct input data and controlled experiments for validation.

REFERENCES

1. *A Comparison of Efficient Beamforming Algorithms*, R.A. Mucci, IEEE Transactions on Acoustics, Speech, and Signal Processing, June 1984, Vol. 32, Iss. 3, pg. 548-558.
2. *What is Synergic MIG/MAG Welding*, <www.twi-global.com>, Accessed 11 October 2016.
3. *Department of Defense Design Criteria: Welded Joint Design*, MIL-STD-22D, 29 August 1979.
4. D. C. Hart, *5xxx Aluminum Sensitization and Application of Laminated Composite Patch Repairs*. In: G. Cloud, E. Patterson, and D. Backman (eds), Joining Technologies for Composites and Dissimilar Materials, Volume 10, Conference Proceedings of the Society for Experimental Mechanics Series (CPSEMS) Book Series, Springer Cham (2017).
5. G. Margelowsky and A. Brock, *Three-Dimensional Distortion Measurements of 5456 Aluminum Due to Synergic Gas Metal Arc Welding*, Naval Surface Warfare Center, Carderock Division (NSWCCD) Technical Report, NSWCCD-65-TR-2015/36, November 2015.
6. *Guide for Verification and Validation in Computational Weld Mechanics*, American Welding Society (AWS) A9.5, 2013.
7. J. Gilbert Kaufman, *Properties of Aluminum Alloys - Tensile, Creep & Fatigue Data at High and Low Temperatures*, ASM International, 1999.
8. J. Gilbert Kaufman, *Fire Resistance of Aluminum and Aluminum Alloys,* ASM International, 2016.
9. *Al 5052-H34*, Visual-Weld 2015 Material Database, ESI Group.
10. *Alloy 5556 Weld Data Sheet*, AlcoTec Wire Corporation, < http://www.alcotec.com>, Access 20 November 2017.
11. R. Beygi, E. Marques, L. F.M. da Silva, *Computational Concepts in Simulation of Welding Processes*, Series: Springer Briefs in Applied Sciences and Technology, Springer Cham, 2022.
12. J. Goldak, A. Chakravarti, and M. Bibby, *A New Finite Element Model for Welding Heat Sources*, Metallurgical Transactions B, Vol. 15, 1984, pg. 299-305.
13. J. N. DuPont and A.R. Marder, *Thermal Efficiency of Arc Welding Processes*, Welding Journal, Vol. 74, No. 12, 1995, pg. 406-416-s.
14. *Aluminum – Vol. 1: Properties, Physical Metallurgy, and Phase Diagrams*, ed. K.R. Van Horn, American Society for Metals, Metals Park, OH, 1967.
15. M. J. Dantin, J. K. Semple, S. M. Orzolek, and C. R. Fisher, *Fabrication Data Elements to Inform Modeling and Simulation of Metal-based Welding and Additive Manufacturing Processes*, Naval Surface Warfare Center, Carderock Division (NSWCCD) Technical Report, NSWCCD-61-TR-2023/03, July 2023.

This page intentionally left blank

DISTRIBUTION

EXTERNAL

	Copies
DEFENSE TECHNICAL INFORMATION CENTER 727 JOHN J KINGMAN ROAD SUITE 0944 FORT BELVOIR, VA 22060-6218	1
RESEARCH COMMONS NAVAL UNDERSEA WARFARE CENTER BUILDING 101 NEWPORT, RI 02841	1
CHIEF OF NAVAL RESEARCH ATTN: CODE 332 OFFICE OF NAVAL RESEARCH 875 NORTH RANDOLPH STREET ARLINGTON VA 22217 ATTN: Farren, Mullins	2
COMMANDER ATTN: SEA 05P2 NAVAL SEA SYSTEMS COMMAND 1333 ISAAC HULL AVENUE S.E. WASHINGTON NAVY YARD WASHINGTON, DC 20376 ATTN: Archer, Bjornson, McGrorey, Melvin	4

NSWCCD INTERNAL DISTRIBUTION

Code	*Name*	*Copies*
60		1
60	Mercier	1
60	Rivera	1
60	Hovanec	1
604	Waters	1
61	DeLoach	1
611	Davis	1
611	Bechetti	1
611	Chen	1
611	Dantin	1
611	Fisher	2
611	Semple	1
611	Sinfield	1
618	Vail	1
653	Brock	1
653	Margelowsky	1


NAVSEA
WARFARE CENTERS
Carderock